Novaya Zemlya effect and sunsets

Siebren Y. van der Werf, Günther P. Können, and Waldemar H. Lehn

Systematics of the Novaya Zemlya (NZ) effect are discussed in the context of sunsets. We distinguish full mirages, exhibiting oscillatory light paths and their onsets, the subcritical mirages. Ray-tracing examples and sequences of solar images are shown. We discuss two historical observations by Fridtjof Nansen and by Vivian Fuchs, and we report a recent South Pole observation of the NZ effect for the Moon.

OCIS code: 010.4030.

1. Introduction

The image of the low Sun that we see depends critically on the temperature profile in the lowest few hundred meters above ground or sea level. For a standard temperature profile, with a constant temperature gradient, the Sun just flattens but is not otherwise distorted.

When there is in addition a warm surface layer over the ground or the water, an observer above this layer may see an inferior mirage, the desert mirage: A second image of the Sun appears below the first and looks like its reflection. As the Sun sinks lower, the two images merge together to form the familiar omega shape, and finally the Sun's last light disappears in a green flash.

Cold surface layers can produce various forms of distortion. The most dramatic example is the Novaya Zemlya (NZ) effect, an arctic mirage over huge distances, caused by a strong temperature inversion. Here the image of the Sun may be rectangular and can be split into several horizontal pieces.

To understand these effects and to reproduce them by calculation, one has to know how the refraction varies with the apparent altitude. Given a model of the atmosphere that allows the refractive index to be found for all heights, the refraction can be established by means of tracing the light's path backwards from the eye of the observer to the object from which it was emitted. In this paper we present such models and the ray-tracing calculations that go with them.

The emphasis of the present analysis will be on the NZ mirage. To show how the NZ mirage fits in the family of sunsets, we shall also discuss the standard atmosphere and the desert mirage.

Ray-tracing calculations are based on the curvature of the light's path, defined as the inverse of its radius of curvature: $c \equiv 1/r$. However, for the sake of discussion we find it convenient to express the curvature in a local Cartesian frame and measure height from the Earth's surface upwards and the horizontal coordinate as distance along it. We show in Section 2 that for near-horizontal rays this terrestrial ray curvature is just $c_T = 1/r + 1/R_E$, where R_E is the Earth's radius.

For a normal atmosphere, the temperature gradient is approximately -0.006 °C/m, and the light's radius of curvature is ~6 times larger than that of the Earth. Upon backward tracing, a ray that is horizontal at the observer's position is bent downwards, but the Earth's surface curves away faster, and the ray escapes. To the observer, c_T is then positive, and he would say that the ray is bent away from the Earth.

When, however, there exists a strong temperature inversion, where in some height interval the vertical temperature gradient exceeds the value of 0.11 °C/m, c_T becomes negative in that interval, and near-horizontal light rays in this region are bent back towards the Earth. This may give rise to oscillatory light paths, which is the characteristic of the NZ mirage. In the following we shall use the phrases NZ mirage and NZ effect indiscriminately.

We discuss the NZ mirage for the situation of an

S. Y. van der Werf (vdwerf@kvi.nl) is with the Kernfysisch Versneller Instituut, University of Groningen, Zernikelaan 25, 9747AA Groningen, The Netherlands. G. P. Können (konnen@knmi.nl) is with the Royal Netherlands Meteorological Institute, P.O. Box 201, 3730AE de Bilt, The Netherlands. W. H. Lehn (lehn@ee.umanitoba.ca) is with the Department of Electrical and Computer Engineering, University of Manitoba, Winnipeg R3T 5V6, Canada.

Received 29 November 2001; revised manuscript received 20 March 2002.

0003-6935/03/030367-12$15.00/0

observer below and above the inversion and distinguish these two situations as the superior and the inferior NZ mirages, respectively. In addition, we study the onsets to these effects, which we denote as subcritical NZ effects, and finally we investigate their color dispersion. The subcritical inferior mirage has been named the "mock mirage" by Young *et al.*[1]

Most of the classical observations (Barents,[2,3] Nansen,[4] Shackleton[5]) were doubtlessly made for an overhead inversion and should be classified as superior mirages. In this paper we give a short discussion of the observations of Nansen and of the less-known observation of Sir Vivian Fuchs,[6] made on 14 August 1957 at Shackleton Base. The latter case may well have been an example of an inferior NZ mirage. An extensive analysis of Barents' observation, made on Novaya Zemlya in 1597, is presented in a separate paper in this issue.[7]

This paper is organized as follows: Section 2 deals with ray tracing and the description and parametrization of the atmosphere. In Section 3 we make a rough classification of the different types of sunset and indicate how the NZ effect fits into this family. Section 4 gives a more detailed analysis of both the superior and the inferior NZ mirages. The observations of Nansen and Fuchs are discussed in Section 5. In Section 6 we present the first recording of the NZ effect for the Moon, an observation made at U.S. Amundsen–Scott South Pole Station on 7–8 May 1998. Section 7 contains a summary. In order not to interrupt the reading, the derivation of some equations that are less commonly known or used are deferred to Appendix A.

2. Model of the Atmosphere and Ray Tracing

The techniques used in this paper are the same as used by Van der Werf.[8] Here we generalize these procedures so that they will be applicable to nonstandard atmospheres that also have horizontal temperature and pressure gradients. Below we sketch these generalizations. Derivations are given in Appendix A.

The backward ray-tracing procedure is illustrated in Fig. 1. It requires that one should be able to evaluate the curvature at any arbitrary point P of the ray. The curvature of a light ray in the atmosphere is proportional to the logarithmic gradient of the refractive index, n. When this depends not only on height, h, but also on x, the distance along the Earth's surface, one has at P with polar coordinates (R, ϕ) (see Appendix A),

$$\frac{1}{r} = \frac{1}{n(h, x)}\left[\cos(\beta)\,\frac{\partial n(h, x)}{\partial h} - \sin(\beta)\,\frac{\partial n(h, x)}{\partial x}\right], \tag{1}$$

where r is the light ray's radius and $\beta = \arctan(\mathrm{d}h/\mathrm{d}x)$ is the tilt of the ray relative to the local horizontal. The curve is concave relative to the Earth's center when $r < 0$, convex when $r > 0$.

In a local Cartesian coordinate frame, where h and x are distances above and along the Earth's surface, the light ray's curvature is given by

$$c_T(h, \beta) \equiv \frac{\mathrm{d}^2h/\mathrm{d}x^2}{[1 + (\mathrm{d}h/\mathrm{d}x)^2]^{3/2}} = \frac{1}{r} + \frac{1}{R}\cos(\beta)[1 + \sin^2(\beta)], \tag{2}$$

where $R = R_E + h$. In the following we shall call this the terrestrial ray-curvature. For near-horizontal rays, close to the Earth's surface the rays obey to a good approximation the relation

$$\frac{\mathrm{d}^2h}{\mathrm{d}x^2} \approx \frac{1}{r} + \frac{1}{R_E} = c_T(h, \beta = 0). \tag{3}$$

In this study we shall be concerned with rays that are always very nearly horizontal, and in the following we shall often abbreviate the terrestrial ray-curvature's notation to just c_T, understanding that it still depends on height.

Exact ray-tracing calculations are most easily performed in polar coordinates (R, ϕ) around the Earth's center. Any curve obeys[8]

$$\frac{\mathrm{d}R}{\mathrm{d}\phi} = R\,\tan(\beta), \tag{4}$$

$$\frac{\mathrm{d}\beta}{\mathrm{d}\phi} = 1 + \frac{1}{r}\,\frac{R}{\cos(\beta)}. \tag{5}$$

As above, β is the tilt angle of the ray relative to the local horizontal, or, stated differently, it is the complement of the angle between the position vector and the curve at the point (R, ϕ).

Equations (4) and (5) form a system of two coupled first-order differential equations for R and β with ϕ as independent variable. They are amenable in this

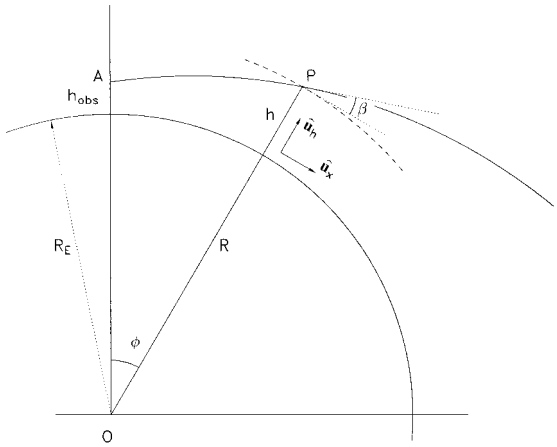

Fig. 1. Illustration of the ray-tracing procedure. The observer is in A at height h_{obs} above sea level. The ray enters from the right and passes through point P, with polar coordinates (R, ϕ) at height h above sea level, where its angle with the local horizontal is β. At P a local frame of reference is defined with unit vectors $\hat{\mathbf{u}}_x$ (horizontal) and $\hat{\mathbf{u}}_h$ (vertical).

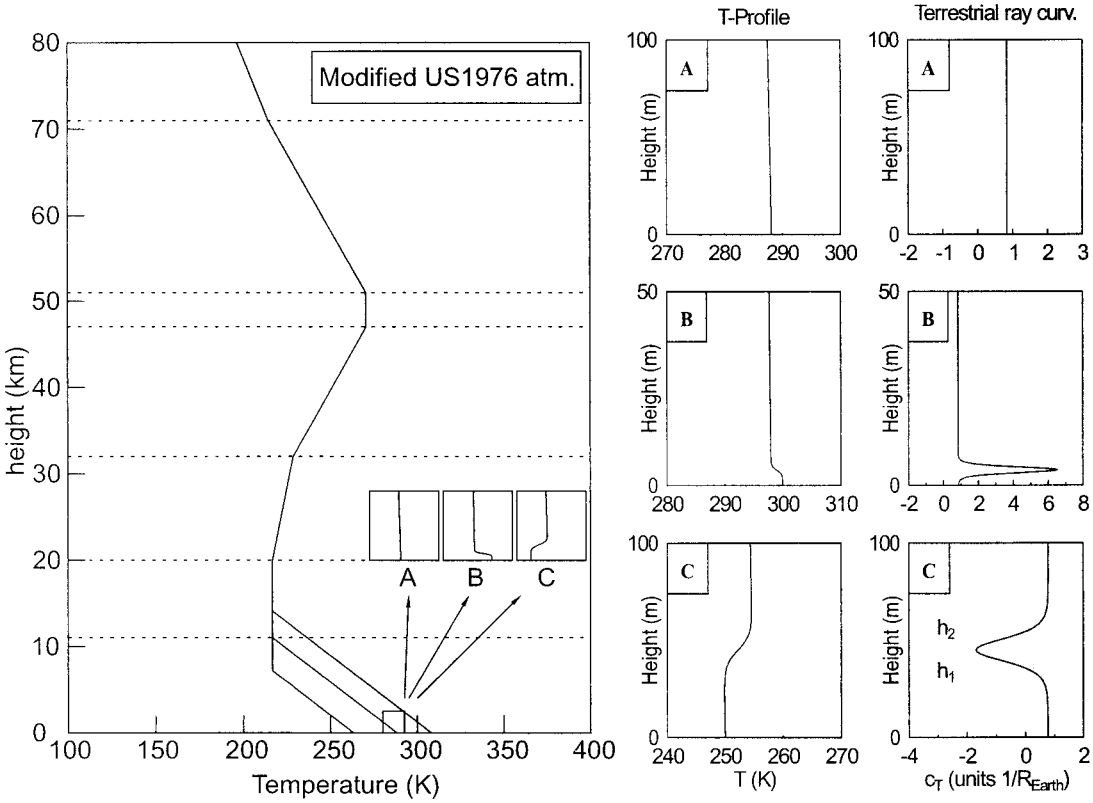

Fig. 2. Left, the modified US1976 atmosphere, shifted in the troposphere to match the sea-level temperature. At low heights an additional temperature profile may be added, indicated by the insets and shown enlarged in the middle diagrams: A, standard atmosphere, sea-level temperature $T_0 = 288.15$ K (15 °C). B, a warm layer as could produce a desert mirage for an observer above it. $T_0 = 300.15$ K (27 °C), $h_{ciso} = 4$ m, $a = 0.5$ m, and $\Delta T = -2$ °C. C, a cold layer as could produce the NZ effect. $T_0 = 250.15$ K (−23 °C), $h_{ciso} = 45$ m, $a = 4$ m, and $\Delta T = 5$ °C. The diagrams on the right show the corresponding terrestrial ray-curvatures in the lower atmosphere for near-horizontal rays.

form to numerical integration, e.g., by the fourth-order Runge–Kutta method, under the condition that in every point the radius of curvature, $r = r(R, \beta, \phi)$, can be evaluated.

This scheme is more general and flexible than the conventional method of Auer and Standish[9] and needs no additional provisions to handle negative apparent altitudes and oscillatory ray trajectories. Moreover, it may be used without modifications when the atmosphere exhibits horizontal temperature and pressure gradients, such as we shall need in this paper.

The index of refraction, n, follows from (see Appendix A)

$$n(h, x) = 1 + \frac{A(\lambda)P(0, x)}{T(h, x)} \times \exp\left[-B\int_0^h \frac{g(h')}{g(0)}\frac{dh'}{T(h', x)}\right]. \quad (6)$$

Here, $T(h, x)$ is the temperature profile; $P(0, x)$, the atmospheric pressure at sea level; and $g(h)$, the gravitational acceleration at height h. $A(\lambda)$ depends slightly on wavelength. Using the wavelength dependence of dry air as given in the *Handbook of Chemistry and Physics*,[10] one finds the following values for green, yellow, and red light: $A(520\text{ nm}) = 7.8998\ 10^{-5}$ K/hPa (green), $A(580\text{ nm}) = 7.8686\ 10^{-5}$ K/hPa (yellow), and $A(650\text{ nm}) = 7.8434\ 10^{-5}$ K/hPa (red). Further, $B = 3.4177\ 10^{-2}$ °C/m.

To find $n(h, x)$, it is necessary to have a functional description of $T(h, x)$ that will be suitable for ray tracing and flexible enough to describe the characteristics of the atmospheres that cause the NZ effect and the desert mirage. We use a temperature profile that is based on the U.S. standard atmosphere of 1976 (US1976). To allow for a free choice of the temperature at sea level, T_0, the height of the troposphere, H_T, is made variable. Also, the atmospheric pressure at sea level, P_0, is made adjustable. The thus modified US1976 atmosphere has been denoted as MUSA76.[8] We may append to this MUSA76 atmosphere a warm or cold layer, for which we use an analytical form, borrowed from the theory of the electron gas, where it is known as the Fermi distribution. The same function is used in nuclear physics, where it is encountered as the Woods–Saxon potential:

$$T(h, x) = T_{MUSA76}(h) - \Delta T(x) + \frac{\Delta T(x)}{1 + \exp\{-[h - h_{ciso}(x)]/a(x)\}}. \quad (7)$$

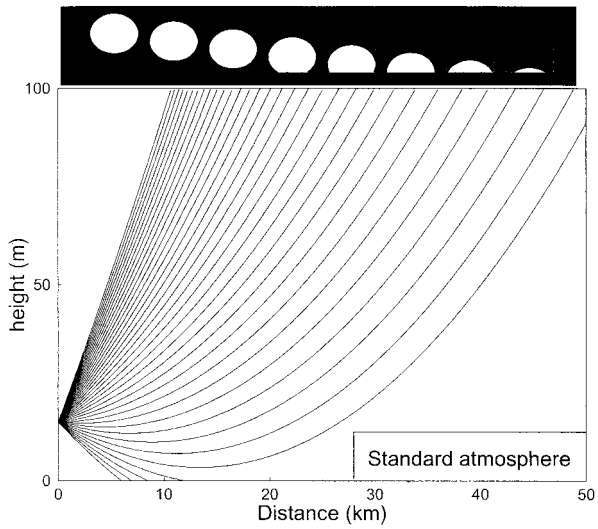

Fig. 3. Light paths for the standard atmosphere (inset A of Fig. 2) traced backwards from an observer's height at 15 m, up to an apparent altitude of 50′. The corresponding images of the Sun are shown along the top, for equidistant steps in altitude. The scale of the horizontal distance along the Earth (x axis) has been compressed by a factor 500 relative to the y axis.

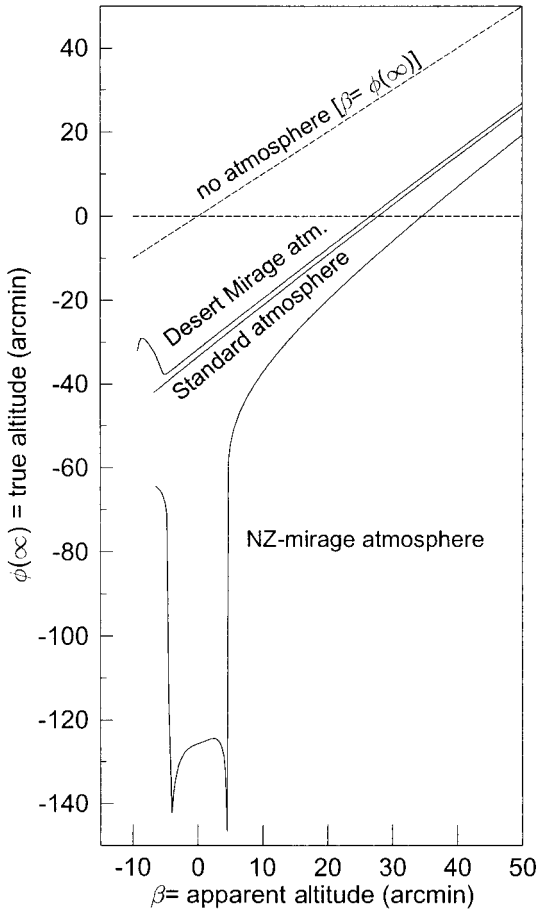

Fig. 4. Transformation curves for the standard atmosphere, the desert mirage atmosphere and the NZ mirage atmosphere shown in Fig. 2, for an observer at $h = 15$ m. If there were no atmosphere, the true and the apparent altitudes would be equal (upper curve).

Here, $h_{\mathrm{ciso}}(x)$ is the height of the isotherm about which the added temperature profile is centered. $\Delta T(x)$ is the temperature jump across the inversion, and the diffuseness parameter $a(x)$ determines the width of the jump.

Figure 2 shows the MUSA76 atmosphere. The insets, shown enlarged in the second column, indicate the cases of A, no addition; B, an additional warm layer; and C, an additional cold layer. The corresponding terrestrial ray-curvatures are shown in the third column.

3. Rough Classification of Sunsets

The image of the Sun can be found when for each true (geometric) altitude, $\phi(\infty)$, the apparent altitude, β, is known. The functional relationship between them can be named the transformation curve.

A rough classification of sunsets is made in this section, taking as examples the three temperature profiles shown in Fig. 2. For each of them we give an example of ray tracing, the transformation curve, and a sequence of images for the setting Sun. All ray tracings are done up to a height of 85 km.

If there were no atmosphere at all, the path of a light ray would be straight and a light-emitting body would be in the direction in which it is seen. The transformation curve would be simply given by $\beta = \phi(\infty)$. The image of the Sun would be perfectly round, progressively chopped off from below by the horizon as it sinks.

A. Standard US1976 Atmosphere

Ray tracing for the standard US1976 atmosphere is shown in Fig. 3. The observer's height is 15 m. Light paths for different apparent altitudes are shown in the first 100 m. The pattern is quite regular: Rays do not cross, and the higher the apparent altitude, the higher also the true altitude.

The transformation curve for the standard atmosphere is shown in Fig. 4, along with those for the desert mirage and the NZ effect, discussed in the following subsections. It is depressed relative to the hypothetical case of no atmosphere. The difference between them is the atmospherical refraction, and this increases with decreasing apparent altitude. The latter may become negative because the observer is at a certain height above sea level. The lowest apparent altitude, β_{min}, is the one for which the ray just grazes sea level at its lowest height. This defines the apparent horizon, and $-\beta_{\mathrm{min}}$ is called the horizon dip.

The sequence of the Sun's images on top of Fig. 3 shows a flattening that gives a nearly perfect elliptical shape. The ratio of the vertical and the horizontal axes equals $d\beta/d\phi(\infty)$, which is the Jacobian of the transformation from the true to the apparent altitude. This may in turn be related to the refraction,

which is defined by $\xi \equiv \beta - \phi(\infty)$. It is then convenient to introduce the flattening as

$$\text{flattening} \equiv \frac{\text{hor.axis} - \text{vert.axis}}{\text{hor.axis}} = \frac{\mathrm{d}[\phi(\infty) - \beta]}{\mathrm{d}\phi(\infty)} = -\frac{\mathrm{d}\xi}{\mathrm{d}\phi(\infty)}. \quad (8)$$

Since the refraction increases faster than linear with decreasing true altitude, the flattening increases as the Sun sinks. Its approximate value at apparent altitude $\beta = 0$ can easily be calculated analytically (see Appendix A) and gives, expressed in terms of the terrestrial ray-curvature,

$$\text{flattening}(\beta = 0) \approx 1 - R_E c_T(\beta = 0) = \frac{A(\lambda) P_0 R_E}{T_0^2}\left[\left(\frac{\mathrm{d}T}{\mathrm{d}h}\right)_0 + B\right]. \quad (9)$$

The above equation applies for any atmosphere for which the temperature gradient, $(\mathrm{d}T/\mathrm{d}h)_0$, is constant from sea level up to the height of the observer, under the condition that $0 \le R_E c_T(\beta = 0) \le 1$. Inserting the parameters for the US1976 standard atmosphere, except the temperature gradient, gives

$$\text{flattening}(\beta = 0) \approx 0.21\left[1 + 29.2\left(\frac{\mathrm{d}T}{\mathrm{d}h}\right)_0\right]. \quad (10)$$

For the standard value $(\mathrm{d}T/\mathrm{d}h)_0 = -0.0065$ °C/m, the flattening has a value of 0.17.

B. Desert Mirage

We now consider a warm layer causing a desert mirage. The observer will again be at a height of 15 m above sea level. The parameters are as in Fig. 2, case B: The warm layer has a temperature jump $\Delta T = -2$ °C. The diffuseness is $a = 0.5$ m, and hence more than 90% of this jump is confined in an interval $\Delta h \approx 6a = 3$ m around the central isotherm at $h_{\text{ciso}} = 4$ m [see Eq. (7)]. In the vicinity of this central isotherm the (negative) temperature gradient is so strong that the ratio P/T, and hence the density, increases with height: One has a density inversion. The condition for this to occur is

$$\frac{\mathrm{d}T}{\mathrm{d}h} \le -B = -3.4\ 10^{-2}\ \text{°C/m}. \quad (11)$$

The curvature, $1/r$, then becomes positive, and for the terrestrial ray-curvature, one has $c_T > 1/R_E$, as is shown in Fig. 2, case B.

Rays drawn from the observer's eye at positive apparent altitude travel through an altogether normal atmosphere. But rays seen at negative apparent altitude that come near the density inversion receive an upward sweep in this region, resulting in a smaller refraction. The effect is clear from Fig. 5, which shows that it is possible for rays at negative apparent altitude to cross other rays at less negative apparent altitude.

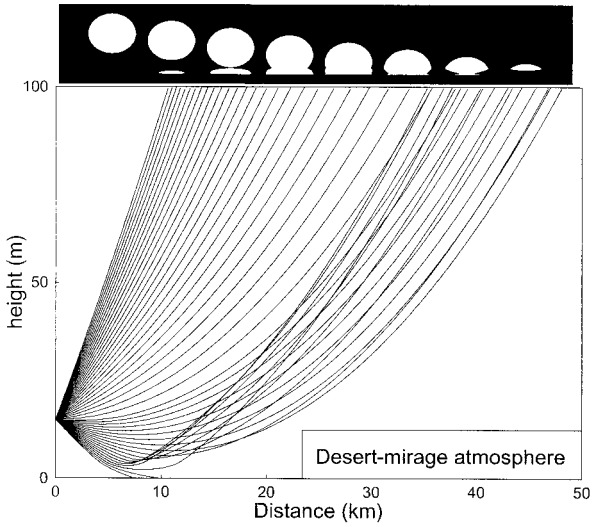

Fig. 5. Light paths for the desert mirage atmosphere (inset B of Fig. 2), observer's height at 15 m, and corresponding images of the Sun in equidistant steps up to 50′ apparent altitude. The desert mirage arises if there is a sufficiently warm layer below the observer (inferior mirage).

The effect of adding a warm surface layer to the (standard) atmosphere on the transformation curve is shown in Fig. 4. The refraction does not increase all the way with decreasing apparent altitude, but suddenly bends upwards again. In this region one has $\mathrm{d}\phi(\infty)/\mathrm{d}\beta < 0$, meaning that the image is mirrored.

The lowest point of the transformation curve marks the vanishing line where the upright image and the mirrored image merge and finally disappear in a point as the Sun sets. This is illustrated by the sequence of images in Fig. 5. The color dispersion is such that the transformation curve for green light lies lower than that for red light. This color dispersion is largest on the vanishing line, and a pronounced green flash may be seen when the air is clean enough.

C. Novaya Zemlya Effect

Next we consider the cold layer as shown in Fig. 2, case C. The observer is again at 15 m above sea level. Overhead for him is a temperature inversion that is centered around $h_{\text{ciso}} = 45$ m. The temperature jump is $\Delta T = 5$ °C, and the diffuseness parameter is $a = 4$ m. Thus, whereas for the desert mirage the observer is above the region of the largest temperature gradient, he now is below it.

From Fig. 2, case C, one notes that the terrestrial ray-curvature, c_T, is negative on a height interval around h_{ciso}. For this to occur, the condition is

$$\frac{\mathrm{d}T}{\mathrm{d}h} > \frac{T(h)^2}{A(\lambda) P(h) R_E} - B, \quad (12)$$

which implies a temperature gradient that is typically larger that 0.11 °C/m.

Denote as h_1 the lowest level in Fig. 2, case C, for which we have $c_T = 0$, so that at $h = h_1$: $1/r = -1/R_E$. Then, by relation (3), and expanding $c_T(h)$ around h_1 up to first order, we have

$$\frac{\mathrm{d}^2(h - h_1)}{\mathrm{d}x^2} = \left(\frac{\mathrm{d}c_T}{\mathrm{d}h}\right)_{h=h_1} (h - h_1). \qquad (13)$$

At $h = h_1$, $(\mathrm{d}c_T/\mathrm{d}h)$ is negative so that relation (12) allows for harmonic oscillations around the height h_1. This solution provides the schematic explanation of the NZ effect.

Figure 6 illustrates the ray-tracing results. Rays of sufficiently high apparent altitude, indicated by A, break through the inversion layer, and the higher β, the less the effect of the inversion. Also rays that, upon backward tracing, start out from the observer on a sufficiently negative altitude will on their upward course pass through the inversion with little disturbance (rays indicated by B). In between there is an interval of β values, symmetric around the true horizon, where the rays enter the inversion zone at small enough angles to be trapped (rays C). They then follow oscillatory paths until the inversion weakens sufficiently that it can no longer sustain the oscillations. The methods for achieving this weakening of the inversion in the context of the ray-tracing formalism are discussed in Section 4.

In the interval of β values, for which the NZ effect occurs, the refraction increases dramatically, and the corresponding true altitudes, $\phi(\infty)$, are much depressed. The transformation curve of the present example is included in Fig. 4.

The images of the sunsets are shown also in Fig. 6. Along the top of the figure one first sees the images of the Sun at positive apparent altitudes (rays A). When β decreases, the part where the rays become oscillatory (rays C) is missing, and the image strongly flattens at the bottom. Next, when the Sun is low enough to match the rays of strongly negative β values (rays B), the corresponding (mirrored) image appears. In between is the gap from which the rays C are missing, which is sometimes called Wegener's blind band.

But when the Sun has sunk far enough, the situation reverses: The rays from categories A and B are now missing, but those from C, which correspond to a much lower true altitude, $\phi(\infty)$, will contribute when the Sun matches these altitudes. This is the depressed part of the transformation curve. The images are highly distorted and pass through a rectangular phase and phases where the image is split into several disjunct components. These are shown in Fig. 6 on the right-hand side.

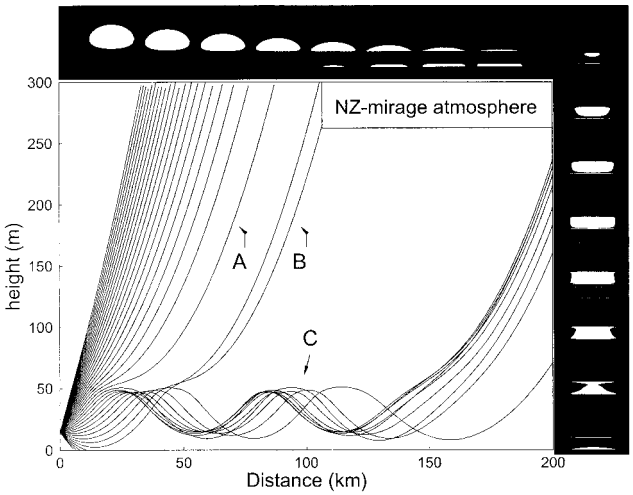

Fig. 6. Light paths for the NZ mirage atmosphere (inset C of Fig. 2), observer's height at 15 m, and corresponding images of the Sun. The strong temperature inversion is here above the observer (superior mirage). For apparent altitudes, β, larger than a given value, the backwards traced rays (indicated by A) break through the inversion. Also, rays of sufficient negative β, which (just) miss the ground, break through the inversion on their upward course (indicated by B). In a limited range of apparent altitudes, around $\beta = 0$, rays follow oscillatory paths (indicated by C). Eventually they escape in a region where the inversion is less strong. The Sun's images on top arise from rays A and B; rays C are missing, which causes the gap. Rays C may produce images when the Sun is well below the horizon (images to the right).

4. Systematics of the Novaya Zemlya Effect

In this section we investigate the NZ effect in more detail. In particular, we study the role of the height of the observer and the strength of the inversion, as embodied in the temperature jump. Also, we study its color dispersion. To do so, we adopt a temperature inversion appended, as before, from the MUSA76 atmosphere. Its central isotherm will be at a height $h_{\mathrm{ciso}} = 40$ m, with a diffuseness parameter of $a = 3$ m. The sea-level temperature is taken as $T_0 = 260$ K in all cases. We shall place the observer below the inversion, at $h = 15$ m and above it, at $h = 45$ m and distinguish these cases as *superior* and *inferior* mirages, respectively. When the temperature jump is strong enough to force at least part of the rays into oscillatory paths, we shall speak of *full mirages*. If the temperature jump is (just) not strong enough to achieve this, we will denote them as *subcritical mirages*.

In its top panels Fig. 7 shows the temperature profile and the terrestrial curvature for such an inversion for a temperature jump of $\Delta T = 5$ °C. The other panels show the tracing examples for the subcritical and full mirages, both inferior and superior.

As mentioned above, it is necessary for a full mirage to let the inversion weaken away from the observer such that the backwards traced rays are allowed to escape upwards through the inversion. There are two obvious ways to achieve this: (1) by making ΔT dependent on distance and making it decrease in a convenient way and (2) by making the diffuseness parameter, a, depend on distance and letting it increase with distance, decreasing in this way the temperature gradient across the inversion. Mathematically, the two methods are rather similar, and we have chosen the second method. For the

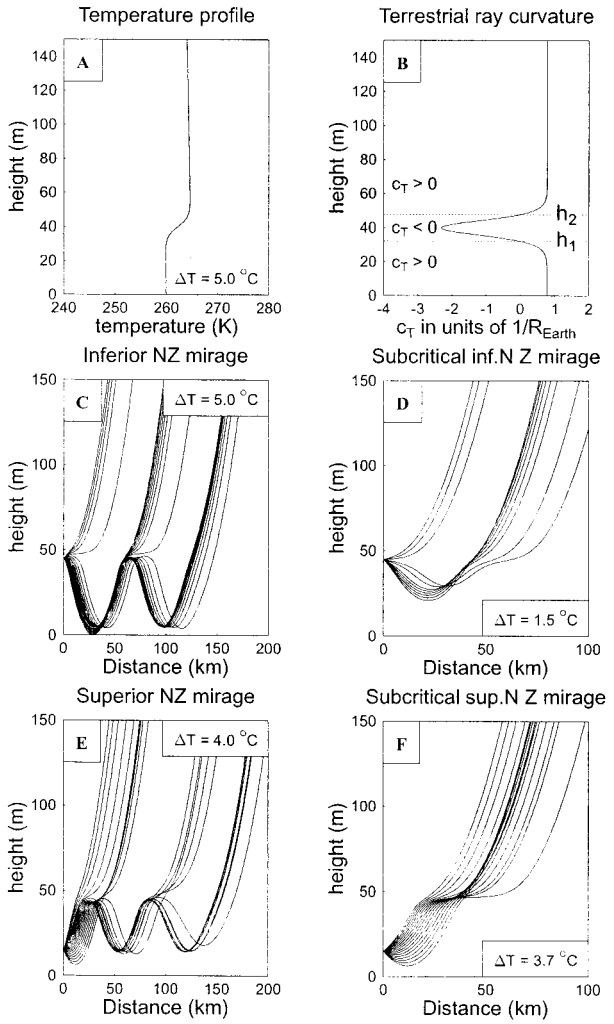

Fig. 7. A, Temperature profile of an inversion, $\Delta T = 5.0$ °C, centered around $h_{\text{ciso}} = 40$ m with a width parameter $a = 3$ m. B, Terrestrial ray-curvature, showing the heights h_1 and h_2, between which c_T is negative. For an observer at $h = 45$ m: C, full inferior NZ mirage, $\Delta T = 5.0$ °C. D, Subcritical inferior NZ mirage, $\Delta T = 1.5$ °C. For an observer at $h = 15$ m: E, full superior NZ mirage, $\Delta T = 4.0$ °C. F, Subcritical superior NZ mirage, $\Delta T = 3.7$ °C.

dependence of the diffuseness on distance we adopt the following form:

$$a(x) = a(0), \qquad x \le x_0, \qquad (14)$$

$$a(x) = a(0)[1 + \alpha(x - x_0)^2], \quad x > x_0, \qquad (15)$$

where x_0 and α are parameters that may be adjusted for each case separately. In all the calculations, shown in this section, x_0 has been set at 50 km. For all subcritical mirages the rays escape already before 50 km, and the value of the parameter α is irrelevant in these cases. However, since α determines how fast the inversion weakens with distance beyond x_0, the ray tracing for the full mirages depends sensitively on its value. The calculations of the full inferior mirage ($\Delta T = 5.0$ °C) and the full superior mirage (for $\Delta T = 4.0$ °C) have been made with a value $\alpha = 0.0001$. For the case of the superior mirage with the much stronger inversion ($\Delta T = 7.0$ °C), $\alpha = 0.0004$ was used.

For an inferior mirage to show oscillatory paths the observer must be within the region where the terrestrial ray-curvature is negative. With reference to Fig. 7B, he must be above h_{ciso} to classify the mirage as inferior, but below h_2, where $c_T = 0$. If he is above h_2, a ray traced backwards starting out at a negative apparent altitude will on its following upward course reach the observer's height again but this time with the opposite apparent altitude and thus escape. If he is, however, below h_2, rays within some range of β values will have oscillatory paths. This range increases as the observer lowers his position.

Also for a superior mirage the height of the observer affects the image. When he has a low position, the ground or sea level limits the range of β values that can be ducted by the inversion to the negative side. But by the same mechanism, also rays at positive apparent altitude are chopped off when, after one oscillation, they return at the observer's height, this time on a downward course. Hence the range of β values that contribute to the image increases with height above the ground.

The transformation curves are shown in Fig. 8 for red (650 nm), yellow (580 nm), and green (520 nm) light. One notes the similarity between the inferior and the superior mirages: For a small temperature jump, such that the mirages are subcritical (Figs. 7D and 7F), rays that are horizontal in the region where the temperature gradient is largest tend to stick to this region. In their transformation curves this effect shows up as a narrow depression, deepening and broadening as ΔT is made to increase. The transformation curves for the subcritical NZ mirages, both superior and inferior, show some similarity to that of the desert mirage (see Fig. 4). Also here, the region of positive apparent altitude, to the right of the depression, gives an upright image. Directly to the left of the dip, the transformation curves slope down and produce an inverted image. In the dip itself the color dispersion is large, especially for the subcritical superior mirage. Both the inferior and the superior mirages, when just subcritical, can produce a pronounced green flash. Typical sunset sequences are shown in Fig. 9.

The subcritical superior and the subcritical inferior NZ mirages also share with the desert mirage the feature that the transformation curves may exhibit a maximum at negative apparent angles. For this to occur the observer should be at a high enough position, else this maximum will be chopped off by the horizon. When the sinking Sun just touches this maximum, it will show the red light first, and the satellite image appears as a red flash.

When ΔT becomes large enough to force some of the rays into oscillatory paths, the dips in the transformation curves are drastically depressed and widened. The regular sunset now has a blind band, as the top row of images in Fig. 6 shows. When the Sun sinks further, it will reappear when its true altitude matches the depressed central part of the

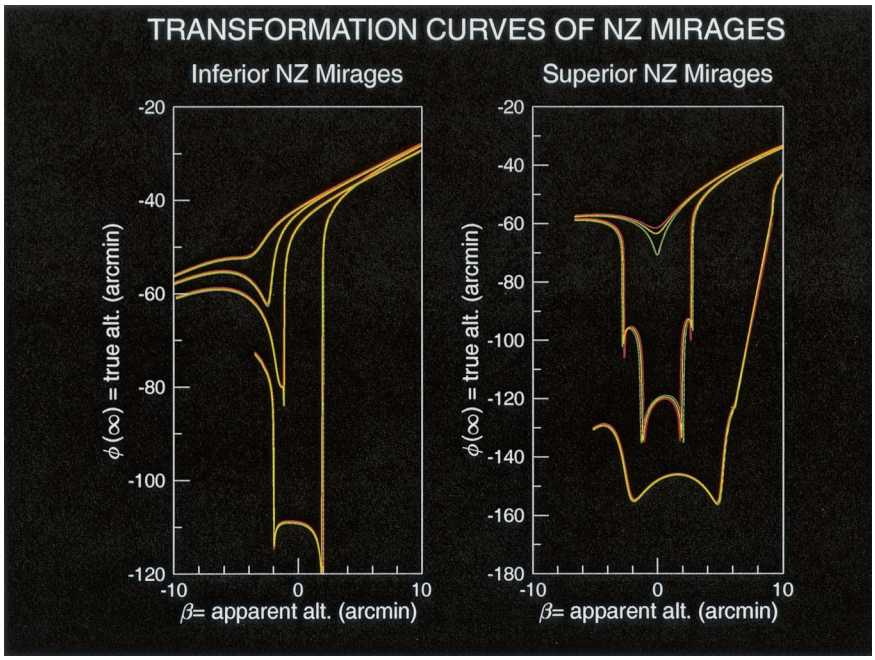

Fig. 8. Transformation curves between apparent altitude and true altitude, for red (650 nm), yellow (580 nm), and green light (520 nm). The vertical axes show the true altitude, $\phi(\infty)$, and the horizontal axes the apparent altitude, β, both in minutes of arc. Left, Inferior NZ mirages for an observer at $h = 45$ m. From top to bottom: $\Delta T = 0.5$, 1.0, 1.5 (subcritical), and 5.0 °C (full mirage). Right, Superior NZ mirages for an observer at $h = 15$ m. From top to bottom: $\Delta T = 3.7$ (subcritical), 4.0, and 7.0 °C. Note the enormous color dispersion of the (just) subcritical superior mirage.

transformation curve, and this time it is seen inside what earlier was the blind band. Also for these full mirages sunset sequences are shown in Fig. 9.

5. The Observations of Nansen and Fuchs

On 16 February 1894 Fridtjof Nansen saw the NZ effect, at 80° 01′ N and approximately 135° E. A drawing, made by him, is shown in Fig. 10. Nansen described it as follows:

> At first the image was a flattened glowing stripe of fire at the horizon. Then two stripes grew out of it, one above the other with a dark space in between. After climbing up the main mast I saw four or even five of such horizontal lines, all equally long such as one would imagine a dull-toned red and square sun, with dark horizontal stripes. (Ref. 4)

The true altitude of the Sun at local noon was −2° 22′. Nansen's description comes close to the images of the superior NZ effect, analyzed before for $\Delta T =$ 7 °C, of which the images are shown in Fig. 9, column 3. The fact that the image grew in width when he climbed up the mast shows that its width was limited by the height of the observer above the ground and, as explained in Section 4, indicates that it must have been a superior mirage.

On 14 August 1957 the NZ effect was observed from Shackleton Base, 77° 57′ S, 37° 17′ W. At local noon the Sun's true altitude was −2° 17′. Fuchs[6] described the event as follows:

> Then a fraction of the sun's disc appeared again, flickered and disappeared. For some time it came and went, the greatest elevation revealing about one tenth of its orb. Sometimes as it reappeared a red flash seemed to shoot out and pulsate along the horizon. (Ref. 6)

Here we possibly have an example of an inferior NZ mirage, at the edge between subcritical and oscillatory. This would explain the small height of the image. See for comparison the images of Fig. 9, fourth column. Further, the observer's position was rather high: 60 m above sea level. And finally, the red flash, "pulsating along the horizon," indicates that the light rays within a small apparent altitude range did skim the ice at the lowest point of their path when going from a subcritical into a full mirage. See also the ray tracing for our analysis of an inferior NZ mirage in Fig. 7C. If the inversion had been overhead, then, for a just critical inversion, the rays would never have come much lower than the height of the observer himself, and could not have been reflected off the ice.

6. Observation of the Novaya Zemlaya Effect for the Moon

On request of one of the authors (G. P. Können), observations on the visibility of the Moon have been made at South Pole Station during the southern winter of 1998. On 7 May 1998 the NZ effect for the Moon was seen, starting at 06:00 UT, when its true altitude was −2° 59′.6. As its declination changed from North to South, the image passed

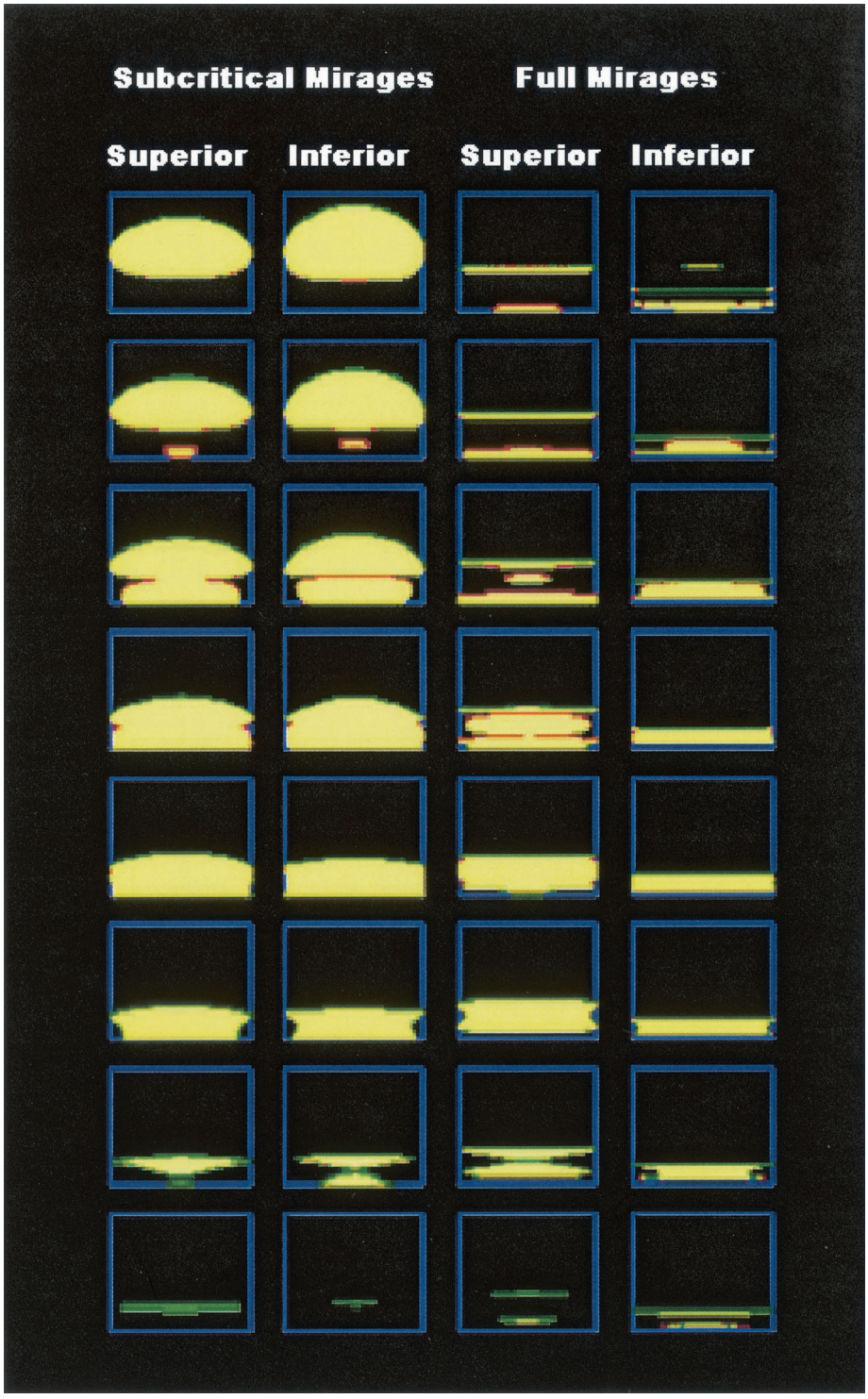

Fig. 9. Images of the Sun for (from left to right) subcritical NZ mirages: superior, $\Delta T = 3.7$ °C (column 1); inferior, $\Delta T = 1.5$ °C (column 2). Full NZ mirages: superior, $\Delta T = 7.0$ °C (column 3); inferior, $\Delta T = 5.0$ °C (column 4). For the subcritical mirages the colors may be realistic; for the full mirages only the red will survive. Note the large green flash in column 1.

through a distorted phase and transformed into its normal appearance at approximately 07:30 UT on 8 May, when its true altitude was 1° 03′.5.

Warmer air was coming in, and the ground temperatures on 8 May were −68 °C (0 UT), −66 °C (6 UT), −60 °C (12 UT) at a pressure of 690 hPa. The temperature inversion was overhead for the observers, and the mirage was of the superior type.

Details of the observation are listed in Table 1. The remarks in the right-hand column are by Rodney Marks. The observer is at 3000 m above sea level. At −68 °C and 690 hPa the astronomical refraction

Fig. 10. Drawing by Fridtjof Nansen of the NZ effect as he observed it on 16 February 1894 at 80° 01′ N and approximately 135° E.

would be 38′.9 for a standard temperature gradient of −0.0065 °C/m and 43′.0 when taken 0 °C/m. This constitutes the first recording of the NZ effect for the Moon.

7. Summary and Conclusions

The Novaya Zemlya (NZ) effect is a mirage that finds its origin in a strong temperature inversion. In its full form, light-ray paths are oscillatory, and a celestial body may become visible even when it is geometrically several degrees below the horizon. We distinguish the paths by the location of the observer relative to the height where the vertical temperature gradient is strongest: For an observer below the inversion, it is a superior mirage, and when the observer is above it, the mirage is of the inferior type. In addition, we have studied the onsets to these effects where the inversion is just not strong enough to force the light rays into oscillation. These mirages have been called subcritical.

It is convenient to discuss sunsets and mirages in terms of the relationship between the true and the apparent altitude, the transformation curve. Knowledge of this transformation curve enables a direct calculation of the shape of the Sun's image. A comparison is made with the sunset under standard atmospheric conditions and with the desert mirage. In all cases the color dispersion has been studied and cases in which the green flash may be expected, identified.

Ray-tracing calculations are at the basis of these transformation curves. We present a general and flexible formalism to perform these calculations and discuss the generalizations that are needed to deal with a nonstandard atmosphere, which also may exhibit horizontal temperature and pressure gradients.

Table 1. Observation of the Novaya Zemlya Effect for the Moon at South Pole Station on 7–8 May 1998

Time (UT, dd/mm)	Declination	Parallax	True Altitude[a]	Remarks[b]
06:00 07/05	2° 05′.5 N	54′.1	−2° 59′.6	Visible
12:00 07/05	1° 08′.5 N	54′.1	−2° 02′.6	Visible
18:00 07/05	0° 11′.3 N	54′.1	−1° 05′.4	Visible
00:00 08/05	0° 45′.9 S	54′.0	−1° 08′.1	Visible
01:30 08/05	1° 00′.2 S	54′.0	0° 06′.2	Flattened, distorted, rippling Observed elevation, ≈2°
06:00 08/05	1° 43′.0 S	54′.0	0° 49′.0	Hardly visible Observed elevation, ≈1°–1°.5
07:30 08/05	1° 57′.3 S	54′.0	1° 03′.5	Regular shape, gibbous phase Observed elevation, ≈1°.5–2°

[a]At South Pole Station: True altitude is −(declination + parallax).
[b]Description by Rodney Marks.

We discuss in some detail the historical observations of the NZ effect of Nansen[4] from 1894 and of Fuchs[6] from 1957. The latter has most likely been the only reported observation of an inferior NZ mirage. Finally, we present some details on the first reported observation of the NZ effect for the Moon, made on 7 May 1998 at South Pole Station.

Appendix A: Mathematical Details and Derivations

1. Curvature in a Nonspherically Symmetric Atmosphere

In the presence of horizontal temperature and/or pressure gradients, also the gradient of the index of refraction will have a horizontal component. One may start from the equation of Born and Wolf:[11]

$$\frac{1}{r} = \frac{1}{n}\,\hat{\boldsymbol{\nu}} \cdot \boldsymbol{\nabla} n, \tag{A1}$$

where $\hat{\boldsymbol{\nu}}$ is a unit vector that is chosen perpendicular on the ray's path. In terms of the local unit vectors $\hat{\mathbf{u}}_h$ and $\hat{\mathbf{u}}_x$, defined at a point P of the path (see Fig. 1), one has

$$\hat{\boldsymbol{\nu}} = \cos(\beta)\hat{\mathbf{u}}_h - \sin(\beta)\hat{\mathbf{u}}_x, \tag{A2}$$

$$\boldsymbol{\nabla} n = \frac{\partial n}{\partial h}\,\hat{\mathbf{u}}_h + \frac{\partial n}{\partial x}\hat{\mathbf{u}}_x, \tag{A3}$$

and this gives Eq. (1) of Section 2:

$$\frac{1}{r} = \frac{1}{n}\left[\cos(\beta)\,\frac{\partial n}{\partial h} - \sin(\beta)\,\frac{\partial n}{\partial x}\right]. \tag{A4}$$

2. Terrestrial Curvature

At a point P on the ray's path with polar coordinates (R, ϕ), one finds from Eq. (4)

$$\beta = \arctan\left(\frac{1}{R}\,\frac{\mathrm{d}R}{\mathrm{d}\phi}\right), \tag{A5}$$

which upon differentiation gives

$$\frac{\mathrm{d}\beta}{\mathrm{d}\phi} = \frac{1}{1 + \left(\frac{1}{R}\,\frac{\mathrm{d}R}{\mathrm{d}\phi}\right)^2}\left[\frac{1}{R}\,\frac{\mathrm{d}^2R}{\mathrm{d}\phi^2} - \frac{1}{R^2}\left(\frac{\mathrm{d}R}{\mathrm{d}\phi}\right)^2\right]. \tag{A6}$$

On the other hand, we know from Eq. (5) that

$$\frac{\mathrm{d}\beta}{\mathrm{d}\phi} = \left[1 + \frac{R}{r}\,\frac{1}{\cos(\beta)}\right] = \left\{1 + \frac{R}{r}\left[1 + \left(\frac{1}{R}\,\frac{\mathrm{d}R}{\mathrm{d}\phi}\right)^2\right]^{1/2}\right\}. \tag{A7}$$

Equating these gives

$$\frac{1}{R}\,\frac{\mathrm{d}^2R}{\mathrm{d}\phi^2} - \frac{1}{R^2}\left(\frac{\mathrm{d}R}{\mathrm{d}\phi}\right)^2 = \left\{1 + \frac{R}{r}\left[1 + \left(\frac{1}{R}\,\frac{\mathrm{d}R}{\mathrm{d}\phi}\right)^2\right]^{1/2}\right\} \times \left[1 + \left(\frac{1}{R}\,\frac{\mathrm{d}R}{\mathrm{d}\phi}\right)^2\right]. \tag{A8}$$

Introducing the differentials $\mathrm{d}R = \mathrm{d}h$ and $R\mathrm{d}\phi = \mathrm{d}x$ in a local frame at P, as shown in Fig. 1, with $\mathrm{d}h$ vertical and $\mathrm{d}x$ horizontal, one finds

$$\frac{\mathrm{d}^2h}{\mathrm{d}x^2} = \left\{\frac{1}{R} + \frac{1}{r}\left[1 + \left(\frac{\mathrm{d}h}{\mathrm{d}x}\right)^2\right]^{1/2}\right\} \times \left[1 + \left(\frac{\mathrm{d}h}{\mathrm{d}x}\right)^2\right] + \frac{1}{R}\left(\frac{\mathrm{d}h}{\mathrm{d}x}\right)^2, \tag{A9}$$

which, when we use $\mathrm{d}h/\mathrm{d}x = \tan(\beta)$ and $[1 + (\mathrm{d}h/\mathrm{d}x)^2]^{1/2} = 1/\cos(\beta)$, gives the terrestrial ray-curvature:

$$c_T(\beta) \equiv \frac{\frac{\mathrm{d}^2h}{\mathrm{d}x^2}}{\left[1 + \left(\frac{\mathrm{d}h}{\mathrm{d}x}\right)^2\right]^{3/2}} = \frac{1}{r} + \frac{1}{R}\{\cos(\beta)[1 + \sin^2(\beta)]\}. \tag{A10}$$

In all practical cases one may then take $R \approx R_E$. When further specializing to near-horizontal rays, for which $\sin(\beta) \ll 1$, this reduces to

$$\frac{\mathrm{d}^2h}{\mathrm{d}x^2} \approx \frac{1}{r} + \frac{1}{R_E} = c_T(h,\, \beta = 0), \tag{A11}$$

which is relation (3) of Section 2.

3. Refractive Index and Temperature Profile

Considering air as an ideal gas, its refractive index is related to the atmospheric temperature, $T(h, x)$, and pressure, $P(h, x)$, by

$$n_\lambda(h, x) = 1 + \frac{A(\lambda)P(h, x)}{T(h, x)}, \tag{A12}$$

where $A(\lambda)$ is the reduced refractivity.[8]

The pressure is related to the pressure at zero elevation, $P(0, x)$, by

$$P(h, x) = P(0, x)\exp\left[-\frac{m}{k}\int_0^h \frac{g(h')\mathrm{d}h'}{T(h', x)}\right], \tag{A13}$$

where k is Boltzmann's constant and m the molecular mass of dry air. The acceleration of gravity varies as

$$g(h) = g(0)\left(\frac{R_E}{R_E + h}\right)^2. \tag{A14}$$

Thus the refractive index is found from

$$n_\lambda(h, x) = 1 + \frac{A(\lambda)P(h, x)}{T(h, x)} \times \exp\left[-B\int_0^h \frac{g(h')}{g(0)}\,\frac{\mathrm{d}h'}{T(h')}\right], \tag{A15}$$

with $B = mg(0)/k = 3.4177\ 10^{-2}$ K/m and for yellow light of 580 nm, $A = 7.8686\ 10^{-5}$ K/hPa.

When we neglect the horizontal components of the gradients of T, P, and n, and replace n in the denominator with 1, the radius of curvature for a near-horizontal ray, close to the Earth's surface, is given by

$$\frac{1}{r} = \frac{1}{n(h)}\frac{\mathrm{d}n}{\mathrm{d}h} = -\frac{A(\lambda)P(0)}{T(0)}\left[\frac{1}{T(h)}\frac{\mathrm{d}T(h)}{\mathrm{d}h} + \frac{B}{T(h)}\right]. \tag{A16}$$

4. Flattening of the Setting Sun

Let an observer be at a height h_0 above sea level. Consider two rays, traced backwards at initial apparent altitudes $\mathrm{d}\beta/2$ and $-\mathrm{d}\beta/2$, hence symmetric around the observer's horizontal. Denote the terrestrial ray-curvature of near-horizontal rays as $c_T \equiv c_T(h = 0, \beta = 0)$.

The light ray at $-\mathrm{d}\beta/2$ will travel an additional distance $\mathrm{d}x = \mathrm{d}\beta/c_T$ before it emerges again at height h_0, but now at an angle $+\mathrm{d}\beta/2$. This follows directly from relation (A11). From there on its path will be identical to that of the ray traced from the observer's position at the positive angle $\mathrm{d}\beta/2$. Hence in true altitude these rays are separated by an angle $\mathrm{d}\phi(\infty) = \mathrm{d}x/R_E$.

Taking the terrestrial ray-curvature, $c_T = 1/r + 1/R_E$ positive and constant over the additional path length $\mathrm{d}x$, which is justified because the ray stays close to the Earth's surface, one finds

$$\mathrm{d}\phi(\infty) = \frac{\mathrm{d}x}{R_E} = \frac{\mathrm{d}\beta}{1 + R_E/r}. \tag{A17}$$

Now $\mathrm{d}\beta/\mathrm{d}\phi(\infty)$ may be identified with the ratio of the apparent vertical and horizontal diameters of the Sun. It is then clear that the Sun appears vertically compressed by a factor $(1 + R_E/r)$. The flattening may defined as [see Eq. (8)]

$$\text{flattening} = 1 - \frac{\mathrm{d}\beta}{\mathrm{d}\phi(\infty)} = -R_E/r. \tag{A18}$$

For a constant vertical temperature gradient $(\mathrm{d}T/\mathrm{d}h)_0$ this gives, with Eq. (A16),

$$\text{flattening} \approx -\frac{R_E}{r(\beta = 0)} = \frac{A(\lambda)P_0R_E}{T_0^2}\left[\left(\frac{\mathrm{d}T}{\mathrm{d}h}\right)_0 + B\right], \tag{A19}$$

which is relation (9).

References

1. A. T. Young, G. W. Kattawar, and P. Parvainen, "Sunset science. I. The mock mirage," Appl. Opt. **36,** 2689–2700 (1997).
2. G. De Veer, *Waerachtige Beschryvinge van drie seylagiën ter werelt noyt soo vreemt ghehoort*, Cornelis Claesz, ed. (Amsterdam, 1598).
3. G. De Veer, *The True and Perfect Description of Three Voyages, so Strange and Woonderfull That the Like Hath Never Been Heard of before*; translation of Ref. 2 by William Phillip, ed. (Pauier, London, 1609).
4. F. Nansen, *Fram over polhavet: den Norske polarfaerd 1893–1896; med en tillaeg af Otto Sverdrup*, H. Aschehoug, ed. (Kristiania, Oslo, 1897).
5. E. Shackleton, *South: The Story of Shackleton's Last Expedition 1914–1917* (MacMillan, New York, 1920).
6. Sir Vivian Fuchs and Sir Edmund Hillary, *The Crossing of Antarctica, The Commonwealth Trans-Antarctic Expedition 1955–1958* (Cassel, London, 1958).
7. S. Y. van der Werf, G. P. Können, W. H. Lehn, F. Steenhuisen, and W. P. S. Davidson, "Gerrit de Veer's true and perfect description of the Novaya Zemlya effect, 24–27 January 1597," Appl. Opt. **42,** 379–389 (2003).
8. S. Y. van der Werf, "Ray tracing and refraction in the modified US1976 atmosphere," Appl. Opt. **42,** 354–366 (2003).
9. L. H. Auer and E. M. Standish, "Astronomical refraction: computational method for all zenith angles," Astron. J. **119,** 2472–2477 (2000).
10. D. R. Lide, *Handbook of Chemistry and Physics*, 81st ed. (CRC Press, Boca Raton, Fla., 2000).
11. M. Born and E. Wolf, *Principles of Optics*, 7th ed. (Cambridge University, Cambridge, UK, 1999).